Dynamical friction in fuzzy dark matter universe

Internship Report

Laboratoire d'Instrumentation et de Recherche en Astrophysique (LIRA), groupe galaxies

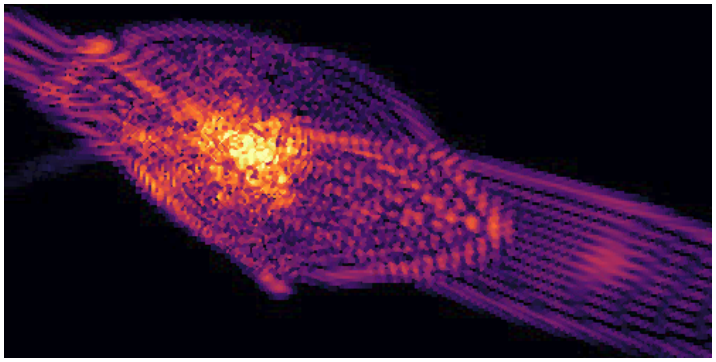

SZPILFIDEL Adrian

Master Sciences de l'Univers et Technologies Spatiales (SUTS)

Observatoire de Paris, Paris Sciences et Lettres (PSL)

Supervisor : BOLDRINI Pierre

July 1, 2025

Acknowledgments

I would like to express my sincere gratitude to Pierre Boldrini for supervising me during my internship and for giving me the opportunity to explore dark matter physics. I am also deeply thankful to the CNES for funding my internship through the Gaia program, which made this valuable experience possible. Lastly, a big thanks to the entire team for making me feel welcome.

Abstract

Context. At cosmological scales, physics is well described by ΛCDM , a model which involves that 27% of the universe is composed of dark matter. The nature of this matter remains unknown so far. Although ΛCDM has been successful, it still has some difficulty matching the observations at galactic scales. One of these deficiencies relates to dynamical friction in dwarf galaxies, which is expected to have caused most of the GCs to fall in the central region of the galaxies. This is not observed in Fornax dwarf galaxy, for instance. A possible answer is to look for alternative cosmological models for dark matter. An exotic model called Fuzzy Dark Matter (FDM) describes dark matter as an extremely light boson particle of mass $m_{\rm FDM} \sim 10^{-22}$ eV. The very low mass of this particle would induce quantum perturbations at galactic scales. Regarding dynamical friction, it is expected for FDM to perturb the dynamical friction, compared with ΛCDM .

Aims. In this work, the main objective is to compare the dynamics of compact objects such as globular clusters that undergo dynamical friction within the dark matter halo, and thus to find in which orbital configurations Cold Dark Matter (CDM) and FDM models are differentiable from each other.

Method. We use orbital integration methods through the code `galpy` to follow the orbits of globular clusters over a long timescale ($\sim$ 10 Gyr). All configurations were tested for energy and angular momentum for gravitationally bound globular clusters in different halos. I developed a new `Python` class for `galpy` to compute the FDM dynamical friction force on orbits.

Results. In CDM halos, using classical dynamical friction, we have restricted the range of energy-angular momentum configurations affected by dynamical friction and found that this depends on the mass ratio of the halo-globular cluster and also on the concentration of the halo. We have noted that the efficiency of dynamical friction is limited by the mass ratio. Above $\frac{\mathcal{M}_{\rm halo}}{M_{\rm obj}} = 10^4$, dynamical friction is no longer efficient in both the CDM and FDM scenarios. For smaller mass ratios, we have found that the FDM model significantly decreases dynamical friction compared to CDM. The magnitude of the difference depends on the mass of the FDM particle, $m_{22} = \frac{m_{\rm FDM}}{10^{-22}{\rm eV}}$. Above $m_{22} \approx 30$, we recover the same dynamics as in CDM universe. Below $m_{22} \approx 0.45$, the FDM dynamical friction is totally inefficient to make the globular clusters spiral down to the center region of the halo.

Contents

Acronyms

CDM Cold Dark Matter. 2, 5, 10, 13–16, 18–21

DF dynamical friction. 5, 7, 8, 10, 11, 13–21

DM dark matter. 5, 6, 8, 11–13, 15, 19, 21

FDM Fuzzy Dark Matter. 2, 3, 5, 8–11, 13–21

GC globular cluster. 2, 5–21

NFW Navarro - Frenk - White. 5, 7, 10, 11, 13–16, 18–21

Introduction

Dark matter (DM) is one of the biggest mysteries and unanswered questions of modern astrophysics. Currently, the ΛCDM model is the dominant cosmological model to describe the evolution of mass-energy in the Universe. The first measurement strongly favorable to ΛCDM has been presented by Riess et al. 1998. The most precise measurements suggest that for a flat Universe, the mass-energy content is mostly composed of matter $\Omega_{\rm m} = 0.315 \pm 0.007$ and dark energy $\Omega_\Lambda = 0.685 \pm 0.007$ (Planck Collaboration et al. 2020). The total matter of the Universe ($\Omega_{\rm m}$) includes baryonic matter and dark matter. This measurement confirmed that baryonic matter only made up 4,9% of the total energy-matter content of the universe. The nature of the dark matter component is still unknown and subject of research. It has been observed that cosmological simulations in ΛCDM scenarios form dark matter halos. The fitted density profile of these halos is now known as Navarro - Frenk - White (NFW) profile (Navarro et al. 1996, Navarro et al. 1997).

ΛCDM has been very successful in describing physics at cosmological scales. It has been tested through various simulations and the predictions are perfectly matched by observations. However, on lower scales, such as the galactic scales ($1 - 100\,\mathrm{kpc}$), it still has issues matching the observations in many cases. For example, Cold Dark Matter (CDM) predicts a number of halos of high mass larger than observed. In addition, the cuspy density profile in the center region of the halos, which is a specific feature of NFW profiles, is not observed. In this work, we are interested in a discrepancy that concerns dynamical friction (DF). DF, first derived in Chandrasekhar 1943, is a key physical process in galaxies responsible for the energy loss of massive objects such as black holes, galaxy satellites, or globular clusters (GCs). An overdensity is formed behind the orbiting object, creating a drag that slows it down. GCs are gravitationally bound spherical systems composed of stars, orbiting around galaxies. They can contain stars from 10^4 to 10^6. These objects are affected by dynamical friction while orbiting within halos. The predicted dynamical friction of the CDM model is too strong in some cases. Let us illustrate this with the example of the Fornax dwarf galaxy. Assuming CDM dynamical friction, Fornax should have disrupted its GCs, and this is not what we observe. Several possible explanations could explain these discrepancies. One possibility is an inaccurate estimation of the (projected) distances. Another explanation could involve baryonic physics, for example. Alternatively, it is also likely that the answer is hidden in the DM nature. A daring DM model, known as Fuzzy Dark Matter (FDM) and first mentioned in Hu et al. 2000, describes dark matter as an extremely light boson of mass $m_{22} = \frac{m}{10^{-22}\mathrm{eV}} \sim 1$. The quantum nature of such a particle cannot be ignored, not even on scales such as galactic scales. This is due to the extreme light mass of this particle that induces quantum effects on galactic scales. On a larger scale ($\sim$ Mpc), the Fuzzy Dark Matter (FDM) model converges to CDM. The quantum effects induced in the halo density will also affect the dynamical friction. Theoretical research has been done on dynamical friction within FDM scenarios in Hui et al. 2017 and Lancaster et al. 2020. They found that the effect of DF is weak compared to classical dynamical friction. This work is a continuation of previous research on FDM dynamical friction. The aim is to extend it to a wide range of orbital configurations, in order to determine under which conditions it is possible to identify effects of FDM physics.

This report is organized as follows. In section 1, I introduce dynamical friction in the classical framework and in the FDM universe. In section 2, I present the method that I used to integrate the orbits and to analyze the effect of dynamical friction. In section 3, I report the results of the effects of dynamical friction in halos and the comparison with FDM. Finally, in section 3.3, I summarize and discuss possible perspectives on this work.

1 Dynamical friction in dark matter halo

1.1 Classical framework

Dynamical friction is a crucial energy loss mechanism in galactic dynamics, especially for objects such as star clusters, black holes, galaxy satellites, or globular clusters. Consider an object of mass $M_{\rm obj}$ orbiting in a gravitational potential formed by a DM or star particles of mass $m_\star$. If we consider $M_{\rm obj} \gg m_\star$, for instance, a globular cluster ($M_{\rm obj} \sim 10^6\,{\rm M}_\odot$) in a galaxy, the object deflects the field particles along its path. This is because, locally, the gravitation force of the object is stronger than the force applied by the galaxy. This deflection creates an overdensity of stars and dark matter located behind the object, resulting in a gravitational force applied backward, and thus a deceleration. This effect will tend the object to fall toward the center of the galaxy potential by loosing energy; this is dynamical friction (see Chandrasekhar 1943, Binney et al. 2008).

The expression of the dynamical friction force is given by the following relation, established by Chandrasekhar 1943 assuming a Maxwellian velocity dispersion :

$$\vec{F} = -\frac{4\pi\mathcal{G}^2 M_{\rm obj}^2 \rho(r)}{v^3} C_{\rm CDM}(r,v)\vec{v} \quad , \tag{1}$$

where

$$C_{\rm CDM}(r,v) = \ln\Lambda \left[{\rm erf}(\frac{v}{\sqrt{2\sigma^2}}) - \frac{2v}{\sqrt{2\pi\sigma^2}} e^{-\frac{v^2}{2\sigma^2}} \right] \quad , \tag{2}$$

$$\ln\Lambda = \ln\frac{r}{\max(r_{\rm hm}, b_{\rm min})} \quad , \tag{3}$$

where $\ln\Lambda$ is the Coulomb logarithm, r is the radial coordinate of the object, $b_{\rm min} = \frac{\mathcal{G}M_{\rm obj}}{v^2}$ the deflection radius of an orbiting object deflected by an angle of 90° and r_{hm} the half-mass radius of the object (about 10 parsecs for GCs), v the velocity of the object, $M_{\rm obj}$ the mass of the object, and $\mathcal{G}$ the gravitational constant. We see that the direction of the deceleration is opposite to the direction of the velocity, which is consistent with what we expected. The force is proportional to the mass of the orbiting object and to the density of the host galaxy, meaning that the dynamical friction is more efficient for a massive object in a denser mass distribution. Looking at the Coulomb logarithm, because we divide by $r_{\rm hm}$, we see that for the same test particle mass, a larger particle's size tends to lower the dynamical friction force. Indeed, dynamical friction is less effective for an extended object because its mass is more diffusely distributed, which makes the gravitational wake less dense.

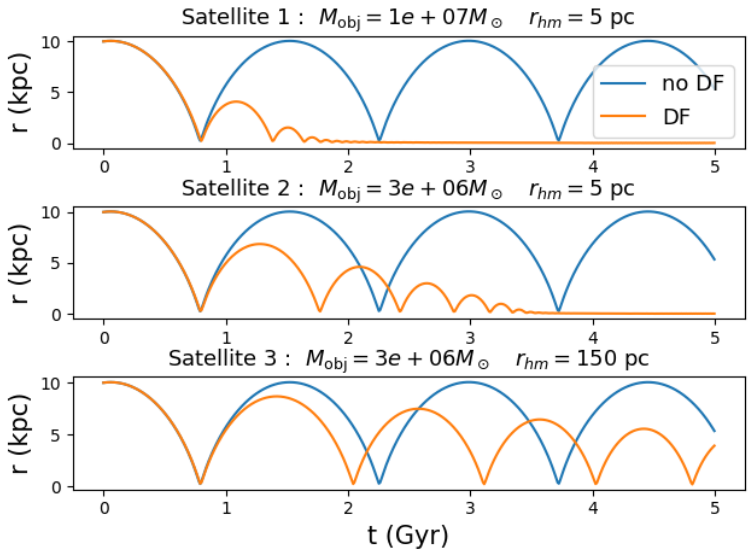

(a) Radial orbits. Radius with respect to time. Each row corresponds to a satellite.

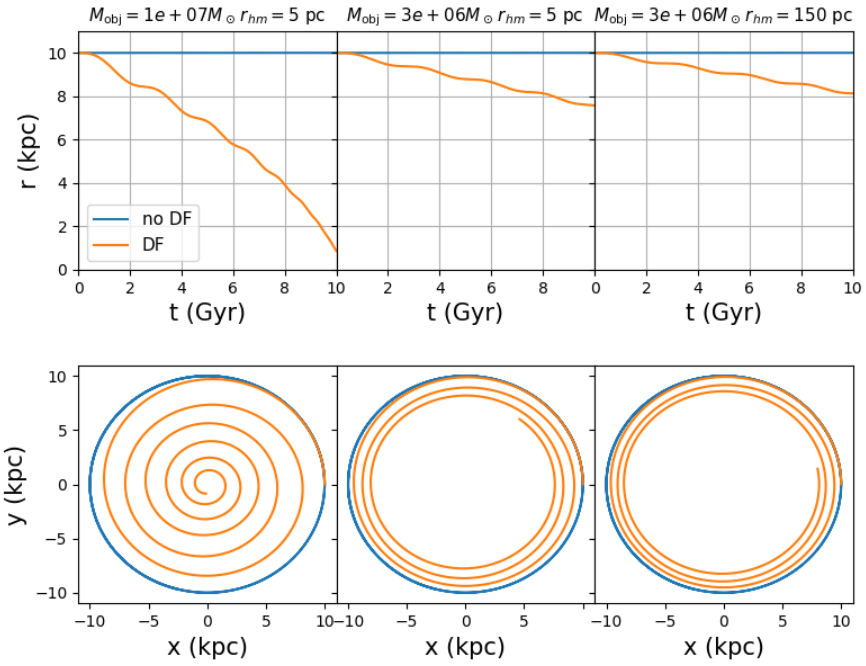

(b) Circular orbits. Columns : each column corresponds to a satellite. First raw : radius of the satellite with respect to time. Second raw : orbit in the xy plane.

Figure 1: Effect of DF on radial and circular orbits. Comparison of orbit with DF (orange curves) and without (blue curve).

Let us look at practical examples to illustrate the effect of dynamical friction on GCs. Consider a NFW halo (Equation 4) of mass $\mathcal{M}_{\rm halo} = 10^9\,{\rm M}_\odot$, scale radius $r_s = 2\,{\rm kpc}$ and virial radius $r_{\rm vir} = 20\,{\rm kpc}$.

$$\rho(r) = \frac{\mathcal{M}_{\rm halo}}{A_{NFW} 4\pi r_s^3 \left(\frac{r}{r_s}\right)\left(1+\frac{r}{r_s}\right)^2}, \tag{4}$$

where $A_{NFW} = \ln(1+c) - \frac{c}{1+c}$, and $c = \frac{r_{\rm vir}}{r_s}$ is the concentration parameter. Then I compare the orbit of 3 different GCs integrated over 5 Gyr. The resulting orbits are represented in Figure 1.

1. Radial orbit (Figure 1a) : We see that without dynamical friction, the GC orbit is independent of its mass and size. The same mass undergoes the same acceleration. But when the dynamical friction occurs, we can see the effect : the GC orbit becomes less elongated and falls to the center; this is because the GC loses energy. This effect increases with the GC mass (comparison between the first and second panels). We observe that more extended objects initiate less dynamical friction (compare the second and third panels). This is because for the same wake, the drag force will be less efficient to slow down all the stars of the GC as it is more extended, its stars are located farther from the wake and, thus, feel a weaker gravitational attraction.

2. Circular orbit (Figure 1b): Again, without dynamical friction (blue curves), the orbits are identical. When adding dynamical friction, the object on the circular orbit starts to spiral toward the distribution center. The dynamical friction is strongly dependent on the mass of the GC for the circular orbit (see the bottom left and bottom center panels). It is slightly affected by the size of the satellite, but the effect is weaker than for radial orbits.

The results of the integrations are very consistent with what we were expecting, according to Chandrasekhar's formula (Equation 1).

1.2 Dynamical friction in Fuzzy Dark Matter halo

FDM model lays on the existence of an ultralight boson ($m_{\rm FDM} \sim 10^{-22}$eV). This extreme light mass is responsible for quantum physics perturbation on the gravitation interaction. As a scale reference for quantum effects, it is relevant to refer to the De Broglie wavelength ($\lambda_{\rm DB} \equiv \frac{h}{mv}$), which gives the characteristic length scale at which quantum effects arise. The De Broglie wavelength of the FDM particle, being inversely proportional to its mass, is therefore very large ($\sim$ kpc), which means that quantum effects affect the halo density. This causes new features to appear in galactic dynamics. There are three main consequences of the FDM model, which can be roughly summarized as follows: it fixes a lower limit on the formation of low mass subhalos; the central region of the DM halo is described by a homogeneous core; and the dynamical friction effect is diminished.

On length scales of the same order as the De Broglie wavelength $\lambda_{\rm DB}$, the equations of motion are modified according to the Schrodinger-Poisson equation. Quantum interferences arise in the gravitational potential, and it creates over- and under- density areas in the DM distribution. This characteristic causes the central density to form a homogeneous core instead of a steep cusp, described by a NFW profile (see Hu et al. 2000, Lee et al. 2010, Boldrini 2021). Also, this has an effect on dynamical friction because the wake density located behind the GC becomes less dense due to interferences. The direct consequence is that the drag force is weaker (Hui et al. 2017). In this work, we specifically look at the effect on dynamical friction. One has to keep in mind that the orbital dynamic of the GC can also be affected by the central core of the mass distribution, which is a feature of FDM halos. However, in this work, we focus on the modification of dynamical friction, without taking into account the cored DM distribution.

The quantum treatment of dynamical friction in the FDM universe leads to a different drag compared to the classical DF developed by Chandrasekhar 1943. The main effect is the reduction of the wake overdensity, decreasing the drag strength. A theoretical work on FDM dynamical friction has been carried out by Hui et al. 2017 followed by Lancaster et al. 2020. It

results in the following relation for the friction force :

$$\vec{F}_{\rm FDM} = -\frac{4\pi\mathcal{G}^2 M_{\rm obj}^2 \rho(r)}{v^3} C_{\rm FDM}(\beta, kr)\vec{v}. \tag{5}$$

The previous relation is analogous to Equation 1 but with a different coefficient $C_{\rm FDM}(\beta, kr)$ that depends on the dimensionless parameter :

$$\beta \equiv \frac{\mathcal{G}M_{\rm obj}m_{\rm FDM}^2}{\hbar^2 k} = k\frac{\mathcal{G}M_{\rm obj}}{v^2} = \frac{kr}{\Lambda}, \tag{6}$$

where $m_{\rm FDM}$ is the FDM particle mass and $k \equiv \frac{m_{\rm FDM}v}{\hbar}$ is the wave number, Λ is the Couloumb logarithm parameter and $\hbar$ is the reduced Planck constant. This parameter β is equivalent to the impact parameter $b_{\rm min}$ encountered in the classical regime multiplied by the wave number k. In this work, we focus on GC orbits.
In this configuration, $kr \sim 1$, and $\frac{\mathcal{M}_{\rm halo}}{M_{\rm obj}} \sim 10^3$, taking the example of the circular orbit :

$$\beta \sim \frac{1}{\Lambda} = \frac{\mathcal{G}M_{\rm obj}}{rv^2} = \frac{M_{\rm obj}}{\mathcal{M}_{\rm halo}} \ll 1. \tag{7}$$

In this regime, the coefficient $C_{\rm FDM}$ reads :

$$C_{\rm FDM}(kr) = {\rm Cin}(2kr) + \frac{\sin(2kr)}{2kr} - 1, \tag{8}$$

where

$${\rm Cin}(z) = \int_0^z \frac{1-\cos(t)}{t}{\rm d}t$$

The expression used to calculate the dimensionless parameter kr is the following :

$$kr = \frac{mvr}{\hbar}. \tag{9}$$

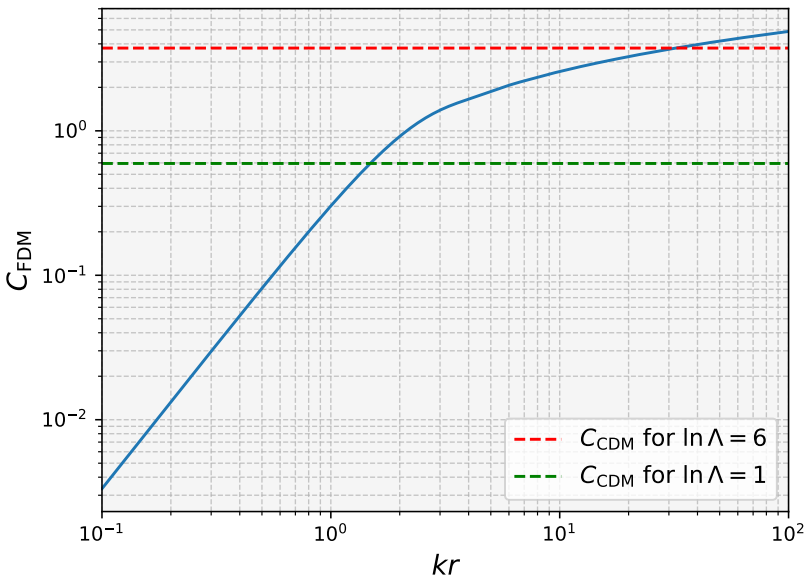

Figure 2: FDM coefficient $C_{\rm FDM}$ (Equation 8) as function of the dimensionless parameter kr. Dashed lines represent classical limits for circular orbits with different values of Λ.

Figure 2 shows that for low values kr, the coefficient $C_{\rm FDM}$ is very low, therefore, it is expected that DF is in the FDM regime. It can be demonstrated that for $kr \ll 1$: $C_{\rm FDM} \to \frac{1}{3}(kr)^2 \propto v^2 r^2$. This limit is reached when $r, v \ll 1$, that is, in the center of the halo. This result injected in (5), using the approximation $\rho(r) \propto r^{-1}$ (NFW near the center), gives :

$$||\vec{F}_{\rm FDM}|| \propto r. \tag{10}$$

In the FDM regime, the closer the object gets to the center of the halo, the lower the dynamical friction. The FDM factor $C_{\rm FDM}$ represented in Figure 2 has an asymptotic behavior for large kr values. For this reason, we use the classical factor described in (2) as a cut-off point, whenever $C_{\rm FDM}$>$C_{\rm CDM}$, so that we ensure that we recover the classical behavior for large kr.

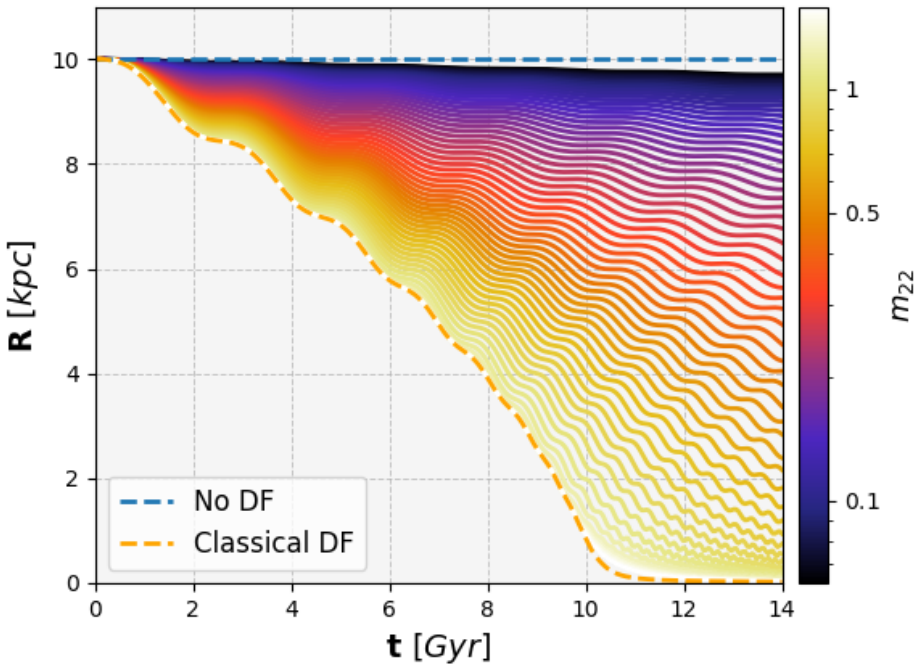

Figure 3: FDM dynamical friction on a circular orbit (same object as the left panel of Figure 1b) in CDM halo, as a function of the value of the mass of the FDM particle m_{22}.

In Equation 8, we notice that the coefficient $C_{\rm FDM}(kr)$ depends on the value of the mass of the FDM particle $m_{\rm FDM}$, since the wave number k is proportional to $m_{\rm FDM}$. A higher value of the mass increases the coefficient $C_{\rm FDM}$, and increases the dynamical friction force (5). On the opposite, lower value of the mass decreases the dynamical friction, and the GC feels a weaker dynamical friction force. We represent an illustration of this effect of the FDM dynamical friction, depending on the value of the particle's mass $m_{22} = \frac{m_{\rm FDM}}{10^{-22}\,\rm eV}$ in Figure 3. We can see for this specific orbit that for $m_{22} \gtrsim 1.5$, we recover the classical regime of DF.

2 Methodology

The present work is based on orbital integration methods using the public code `galpy` (subsection 2.1). In order to cover all possible orbit configurations, it is very meaningful to use energy-angular momentum space (discussed in subsection 2.2). The physical framework of

these numerical integrations as the numerical parameters are given in subsection 2.3. To quantify the dynamical friction effect, we need to fix a disruption criterion to compute the fall-in time of the GC into the center of the host galaxy (subsection 2.4).

2.1 Orbit integration using `galpy`

In order to have control on the physical parameters (such as the halo mass, the dynamical friction, etc.) and huge statistics (we are using 4500 GC orbits per halo), it is convenient to use test-particle simulations, involving static analytical potential. We used the `Python` package `galpy` (Bovy 2015) to perform orbit integration. This public code is adapted to galactic dynamics, it provides an orbit integration tool that uses various analytical potentials. More than 40 different potentials and about 8 integration methods (performed in `Python` and/or C) are available. Thus, we are easily able to create any desired configuration, which is extremely difficult to do using N-body simulations because the number of scenarios and objects are limited by the large calculation time, which can sometimes last for months. We need `galpy` to make large statistics of GCs that undergo dynamical friction within a variety of DM halos. This feature gives to this work a new contribution to GC dynamics, since DF has not been tested on such a large number of orbital configurations. Using `galpy` allows us to integrate 4500 orbits over 10 Gyr in a few seconds, in the physical configuration needed. We have to initialize the gravitational potentials, then set the initial positions and velocities of the orbiting objects, and finally integrate them using the implemented methods.

Although `galpy` provides a large variety of potential classes, such as Chandrasekhar dynamical friction, FDM dynamical friction does not yet exist. So, I built and tested a new class `FDMDynamicalFrictionForce`, which computes the FDM dynamical friction in a similar way to the classical method used in `galpy`. To calculate the FDM friction force, I compute both the classical factor using (2) and the FDM factor using (8). I test whether $C_{\rm CDM}$ is lower or greater than $C_{\rm FDM}$ and keep the lowest for the calculations. This test is necessary to avoid the divergence effects of $C_{\rm FDM}$. This new `Python` class is in the process of being added to the `galpy` package, it will be public and available soon online.

2.2 $E - L_{\rm z}$ space

To characterize an orbit, we use conserved quantities. It is thus very convenient to work in the $E - L_{\rm z}$ space because it allows us to have an overview on all the orbits allowed.

The vertical component of the angular momentum reads:

$$L_{\rm z} = \vec{L}.\vec{e_{\rm z}} = R v_t \quad , \tag{11}$$

where R is the cylindrical radius and v_t the tangential velocity.

The energy of an orbiting object in a spherical distribution is given by :

$$E = \frac{v^2}{2} + \Phi(r) \quad , \tag{12}$$

where $\Phi(r)$ is the gravitational potential. For a NFW profile (see Equation 4), the corresponding gravitational potential is

$$\Phi_{\rm NFW}(r) = -\frac{\mathcal{G}\mathcal{M}_{\rm halo}}{A_{\rm NFW}\, r_s} \frac{\ln(1 + r/r_s)}{r/r_s} \quad .$$

The initial conditions represented in Figure 4 are generated using the following steps :

1. Generate random radii with $r_i \in [0.1 \times r_s,\ 10 \times r_s]$
2. Generate random tangential velocities $v_{t,i} \in [-v_{esc}, v_{esc}]$, where $v_{esc} = \sqrt{-2\Phi_{\mathrm{NFW}}(r)}$.
3. Without losing generality, we can set $z = 0$ and $v_z = 0$, since the potential has spherical symmetry. So the radial velocities, in cylindrical coordinates, read $v_r^2 = v^2 - v_t^2$
4. The random radial velocities are generated with : $v_{r,i} \in [-\sqrt{v_{esc}^2 - v_{t,i}^2}\,, \sqrt{v_{esc}^2 - v_{t,i}^2}]$
5. With the velocities and positions, the initial energies and angular momenta are computed using (12) and (11).
6. We normalize the energy and angular momentum values using their respective values computed for a circular orbit at the scale radius of the halo. We need this normalization to always have the same value of these quantities regardless of the halo parameters used, so that we can directly compare the result in various DM halos.

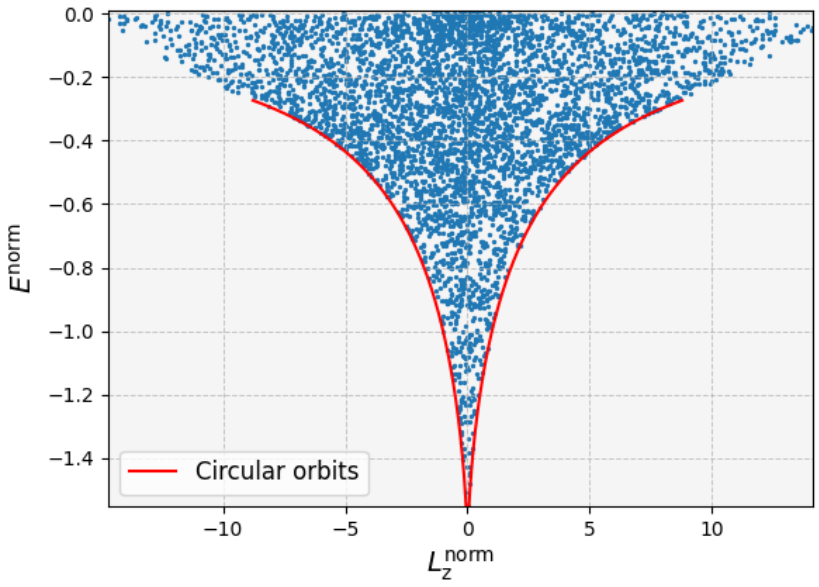

Figure 4: Initial conditions: $E - L_z$ diagram for the initial conditions using 4500 GCs point mass. Horizontal axis: vertical component of the angular momentum, normalized by their absolute values for a circular orbit at the halo scale radius r_s. Vertical axis : orbit energy, normalized by the energy of a circular orbit at r_s. Each dot corresponds to an orbit. The red line corresponds to circular orbits from $0.1 \times r_s$ to $10 \times r_s$.

In a $E - L_z$ diagram, we are interested in bound orbits corresponding to negative energies. Some regions of this diagram are physically forbidden because the kinetic energy is a positive or null quantity, meaning that the total energy of a bound object cannot be lower than the potential energy. These forbidden areas are located on the lower left and right sides of Figure 4. For any orbit with a given angular momentum, the circular orbit corresponds to the minimal energy. Thus, in the $E - L_z$ diagram, the circular orbits are located on the lower red line, delimited by blue dots. To have a good intuition about these diagrams, one has to remember that radial orbits lie on the vertical line at $L_z \sim 0$. The farther away from this value, the more circular the orbit. GCs that are located far from the center are higher in energy and have higher angular momentum.

2.3 Physical framework, parameters and modeling

In `galpy`, a galaxy is modeled as a sum of different potentials (stellar disk, bulge, halo, bar, etc.). We have chosen to run the orbits only in DM halos and not add stellar and gas components. The first reason for this is that it enables us to focus only on the effect of DM, without mixing the effect of baryonic physics that could bias the results. So we properly understand the effect and do not misinterpret the result. The second argument is that we already know that dynamical friction is dominant in dwarf galaxies that are mostly composed of dark matter. Consequently, baryonic matter does not significantly affect the dynamics of globular cluster in dwarf galaxies, so we are not losing realism.

The key parameters characterizing a dark matter halo are its mass ($\mathcal{M}_{\rm halo}$) and its concentration(c). The halo concentration is defined as the ratio between the virial radius, corresponding to the region within which the density is 200 times the critical density of the universe, and the scale radius, which sets the characteristic size of the halo: $c \equiv \frac{r_{\rm vir}}{r_s}$. For a given halo mass, the concentration is determined by cosmological parameters. To ensure realistic values, I use the `colossus` package Diemer 2018 to compute the concentration parameter as a function of the mass of the halo and redshift. `colossus` is a numerical tool widely used in cosmology and the study of large-scale structures and dark matter halos. It provides a straightforward way to calculate the physical properties of dark matter halos within various cosmological models. In this work, all calculations are performed at redshift $z = 0$.

We decided to always keep the same orbiting object: a globular cluster with mass $M_{\rm obj} = 10^6\,{\rm M}_\odot$ and half-mass radius $r_{\rm hm} = 10$ pc, which corresponds to the standard values for GCs. We use the point-mass approximation that is relevant for such dense objects; it would be more difficult to use this approximation for galaxy satellites. Indeed, the internal dynamic of GC can be neglected to integrate its orbit.

Regarding the integration parameters, we decided to always work in the time interval from 0 to 10 Gyr, which corresponds to the lifetime of GC from the early universe to the present time. If a GC survives after 10 Gyr, it is most likely that we can observe it today.

2.4 Fall-in criterion

Since dynamical friction causes the GCs to spiral down, a relevant criterion is to look at whether the object has definitely fallen into the center after the integration time. If it is the case, we can consider the object disrupted, because if we consider globular clusters, for instance, they would undergo a strong tidal force in the center regions, which are the most dense in galaxies.

Therefore, after orbit integration, I compute the time τ from which the satellite has its apocenter smaller than 10% of the scale radius of the dark matter halo, which is of the order of kpc, meaning that the orbit has definitely gone below this distance. Using this condition with $E - L_{\rm z}$ diagram provides a clear idea of where the globular clusters will be after a certain time depending on the orbit's initial conditions in energy and angular momentum.

3 Results

This section is organized as follows. The first subsection 3.1 illustrates the orbit integration of the new code I wrote using FDM dynamical friction and compares it with analytical results. In the following subsections, I compare two scenarios: the first is the CDM scenario, where the halo is described by a NFW halo and the DF by Chandrasekhar formula (1). The second scenario is the semi-FDM, where the halo density profile is still NFW but the DF is computed

using FDM physics. The comparison of the impact of the concentration parameter c on classical DF and FDM DF is presented in subsection 3.2. The comparison of the impact of the halo mass parameter $\mathcal{M}_{\rm halo}$ on classical DF and FDM DF is presented in subsection 3.3.

3.1 Fornax case and comparison with analytical results

In order to test the new `Python` class `FDMDynamicalFrictionForce`, I compared the calculation with the work carried out by Hui et al. 2017. They have computed the orbital time of Fornax GCs using fixed coefficients $C_{\rm CDM}$ and $C_{\rm FDM}$ for dynamical friction using initial conditions given by observations. In this work, I used the same density profiles: the CDM density profile is a NFW profile of scale radius $r_s = 0.8\,\mathrm{kpc}$ and $\mathcal{M}_{\rm halo} = 1.98 \times 10^8\,\mathrm{M}_\odot$, and the FDM profile is a large core profile of scale radius $r_s = 1.4\,\mathrm{kpc}$ and mass $\mathcal{M}_{\rm halo} = 8 \times 10^8\,\mathrm{M}_\odot$ (see Cole et al. 2012). The difference between this work and their is that they only calculated the coefficients for the initial condition, while `galpy` provides a continuously evolving coefficient $C_{\rm CDM}$ (see Equation 2) and $C_{\rm FDM}$ (see Equation 8) that depend on the velocity and position. The result is then more realistic because, as we see in Figure 2, the FDM factor strongly depends on the position and the velocity, which evolve with time. Also, I computed the fall-in time instead of the orbital time that they used. For that, I looked for the time at which the satellite remained below 10% of the scale radius. I compared their orbital time to two fall-in times τ_C and τ. The first fall-in time τ_C is calculated on an orbit integration using a constant $C_{\rm CDM}$ and $C_{\rm CDM}$, that is, using only the value of these coefficients calculated with the initial value of position r and velocity v. The second fall-in time τ is computed on an orbit integrated with evolving coefficients $C_{\rm CDM}(r, v)$ and $C_{\rm CDM}(r, v)$. The result is presented in Table 1 below.

	Radius	GC mass	CDM (Hui +17)		CDM (this work)		FDM (Hui +17)		FDM (this work)	
n	r (kpc)	$m_{\rm cl}$ ($M_\odot$)	$C_{\rm CDM}$	τ_C (Gyr)	τ_C (Gyr)	τ (Gyr)	$C_{\rm FDM}$	τ (Gyr)	τ_C (Gyr)	τ (Gyr)
1	1.85	3.7×10^4	4.29	112	22	25	2.46	215	84	209
2	1.21	1.82×10^5	3.32	9.7	2.15	2.59	1.88	12	6.62	29
3	0.50	3.63×10^5	2.45	0.62	0.22	0.24	0.29	2.2	1.46	11
4	0.28	1.32×10^5	2.50	0.37	0.11	0.15	0.033	10	5.66	18
5	1.65	1.78×10^5	3.46	21.3	4.31	5.12	2.32	31	13	38

Table 1: Table 1 from Hui et al. 2017, updated with the values of coefficients C and orbital time τ computed in this work.

As Hui et al. 2017 have already found, all fall-in times are larger in FDM than in the CDM scenario. This is a compelling result because it means that the FDM dynamical friction is effectively weaker than it is in the classical regime. If we first compare the fall-in time using constant coefficients (τ_C), in both CDM and FDM, with an orbital time of Hui et al. 2017, we see that they are always much smaller. So we find that the orbits fall faster than they were expecting.

In the CDM scenario, the approximation of the constant $C_{\rm CDM}$ is acceptable for our integration, as we see that the fall-in time τ does not differ significantly from τ_C. However, Hui et al. 2017 find very different values that are overestimated, except for GC 4. This means that their calculation is no longer valid for radii larger than at least $r = 0.28\,\mathrm{kpc}$, for a scale radius of $r_s = 0.8\,\mathrm{kpc}$.

On the other hand, we found that in the FDM scenario, this approximation is no longer valid. Indeed, there is a huge gap between τ_C and τ in the FDM column. There are two reasons for this. The first is the DM core stalling effect, which prevents the satellite from entering the halo's core; this effect comes from the cored density profile. The second reason is due to FDM

dynamical friction and is that for low radii, C_{FDM} is also very small, which means that the dynamical friction is no longer efficient. The combination of these two effects maintains the satellite in an almost stable circular orbit.

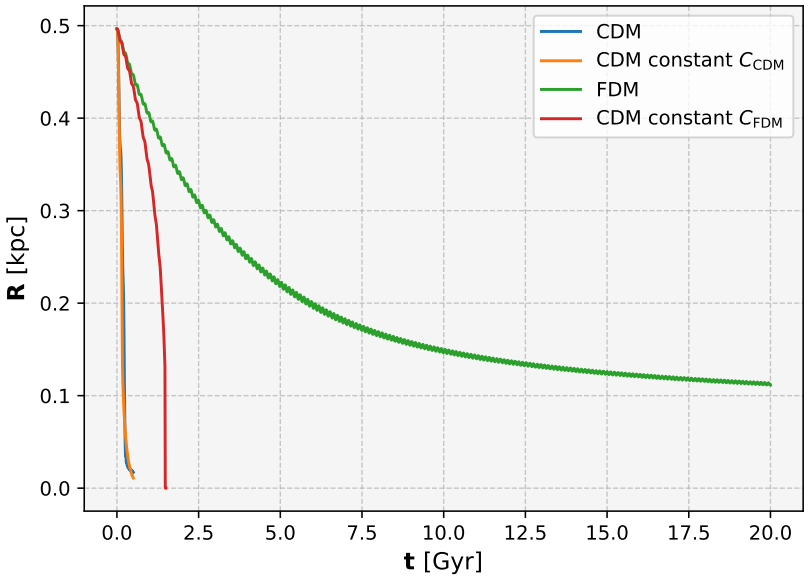

Figure 5: Evolution of the radius of cluster 3 from Table 1. CDM label corresponds to NFW halo + classical DF; FDM label corresponds to Large Core halo + FDM DF.

Figure 5 illustrates the orbital evolution of GC3 where the fall-in time τ is so long compared to τ_C. These effects of core stalling and FDM DF must be taken into account.

3.2 Impact of the concentration parameter c on dynamical friction

Here I present the integration of several GC orbits in the CDM (NFW halo + classical DF) and semi-FDM (NFW halo + FDM DF) scenarios. The results are shown for a $10^9\,\mathrm{M}_\odot$ DM halo with different scale radius r_s values, to highlight the effect of dynamical friction on the orbits, depending on the concentration parameter of the halo ($c = \frac{r_{\mathrm{vir}}}{r_s}$) (see Figure 6). We used 4500 objects to draw the maps; the value of the fall-in time is computed using the median of the values within each hexagon.

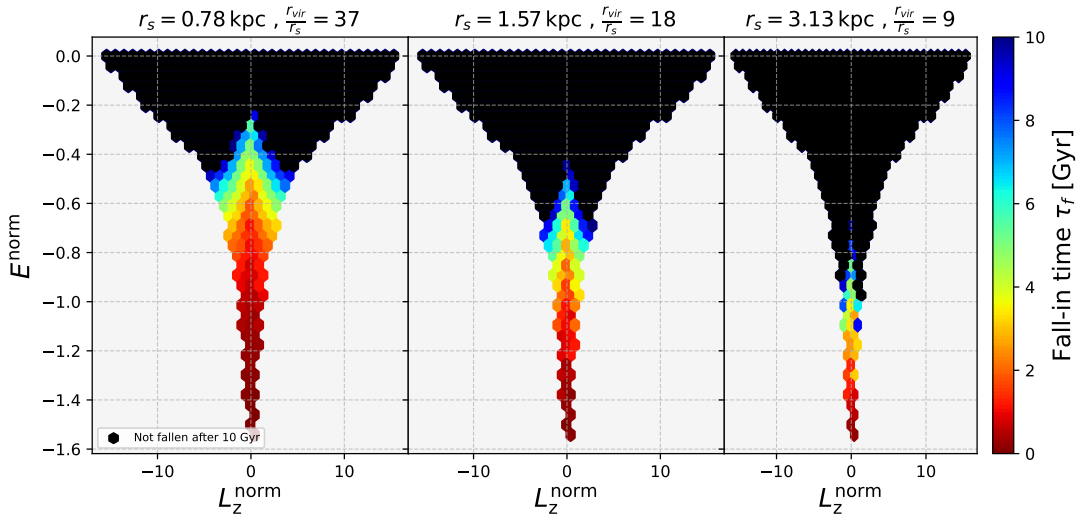

Figure 6: $E - L_z$ diagrams of GC orbits in CDM halos with different scale radius r_s, with a halo-GC mass ratio of 10^3. The quantities have been normalized by their absolute values of circular orbit at the scale radius r_s. The fall-in times are computed using the condition that the radius r of the GC is definitely under 10% of the scale radius r_s.

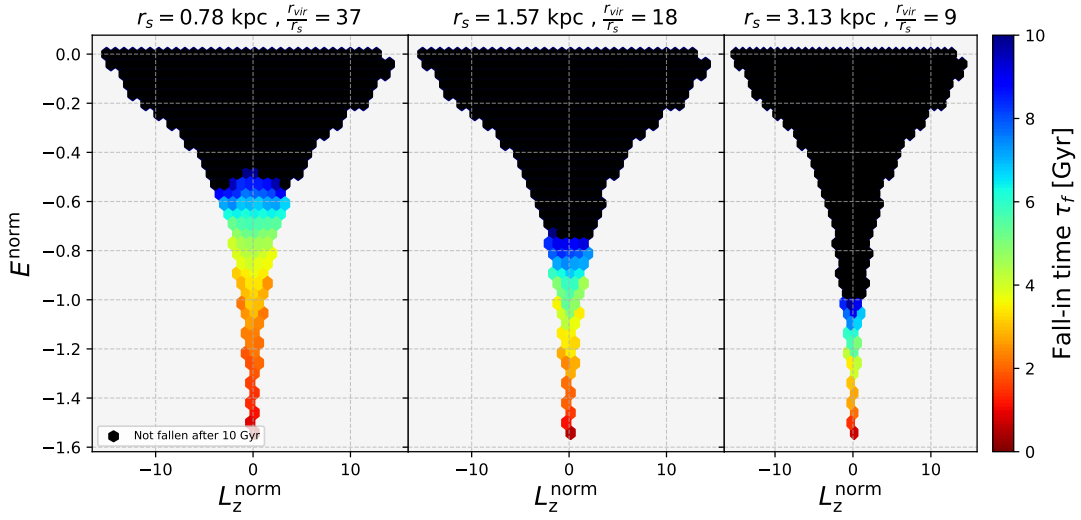

Figure 7: Same as in Figure 6 but integrated using FDM DF, with $m_{22} = 5$.

To investigate the impact of the scale radius on GC orbits, I fixed the mass of the NFW halo to $\mathcal{M}_{\rm halo} = 10^9\,{\rm M}_\odot$, a typical value for dwarf galaxies, and set the GC mass to $10^6\,{\rm M}_\odot$, yielding a mass ratio of 10^3. The scale radius and concentration parameter, calculated using the `colossus` package (see Diemer 2018), are $r_s = 1.57\,{\rm kpc}$ and $c = 18$, respectively; these values correspond to the middle panel of Figure 6.

In the Figure 6, the fate of GCs after 10 Gyr is shown as a function of their initial energy and angular momentum. Surviving GCs (in black) occupy the highest energy states, either because they start with high velocities or are initially far from the center, giving them more energy to lose. For these clusters, DF is not efficient enough to cause them to spiral into the center within 10 Gyr. In contrast, GCs with lower energy, those with lower velocities and/or closer to the center, fall into the center before 10 Gyr. The figure also highlights that radial orbits (vertical line at $L_z = 0$) are more strongly affected by dynamical friction than orbits with the same energy but higher angular momentum. This is expected as radial orbits pass through the densest regions of the halo, where DF is strongest.

Finally, the figure compares the effect of varying the concentration parameter. At fixed virial radius $r_{\rm vir}$, decreasing the scale radius r_s increases the concentration parameter (see Equation 4), resulting in a higher central density. This improves the efficiency of DF, as its strength is proportional to the local density (Equation 1). Conversely, increasing the scale radius lowers the central density and reduces the effectiveness of dynamical friction.

To analyze the impact of fuzzy dark matter (FDM) on the GC orbits, I used the same dark matter halo parameters as in Figure 6: a halo mass of $\mathcal{M}_{\rm halo} = 10^9\,{\rm M}_\odot$ and corresponding concentration values. The difference here is that Figure 7 shows the fall-in times for GCs under FDM dynamical friction, computed using Equation 5 with a particle mass $m_{22} = 5$. This mass was arbitrarily chosen within the expected range, to highlight differences with the classical regime, while ensuring that dynamical friction is not completely suppressed.

Visually, the figure reveals trends similar to those observed in the classical case (Figure 6): GCs with the lowest energies are most affected by dynamical friction, and increasing the concentration parameter enhances the efficiency of dynamical friction, just as in the CDM scenario. However, a key difference is that, for the same halo parameters (mass $\mathcal{M}_{\rm halo}$ and concentration c), FDM dynamical friction is less efficient, GCs take longer to spiral into the center. For example, in the central panel of Figure 7, orbits with normalized energy $E^{\rm norm} \gtrsim -0.8$ do not fall within 10 Gyr, whereas in the classical case, orbits with $E^{\rm norm} \sim -0.4$ already fall in. This trend is consistent across different concentration values: the diagrams are less colored, and the fall-in times are generally longer, illustrating the reduced efficiency of dynamical friction in an FDM universe.

Another notable feature is that, unlike in the CDM scenario, radial orbits are no longer more strongly affected than circular orbits. This can be explained by the fact that, when a GC enters the central region, FDM dynamical friction becomes almost negligible, a distinctive behavior of the FDM regime.

3.3 Impact of the halo-globular cluster mass ratio on dynamical friction

Now, let us see the comparison of orbits dynamic in halos of different masses and, thus, different scale radii. In Figure 8, I report three halo masses, from dwarf galaxy halo ($10^9\,{\rm M}_\odot$) mass to Milky Way halo mass ($10^{12}\,{\rm M}_\odot$).

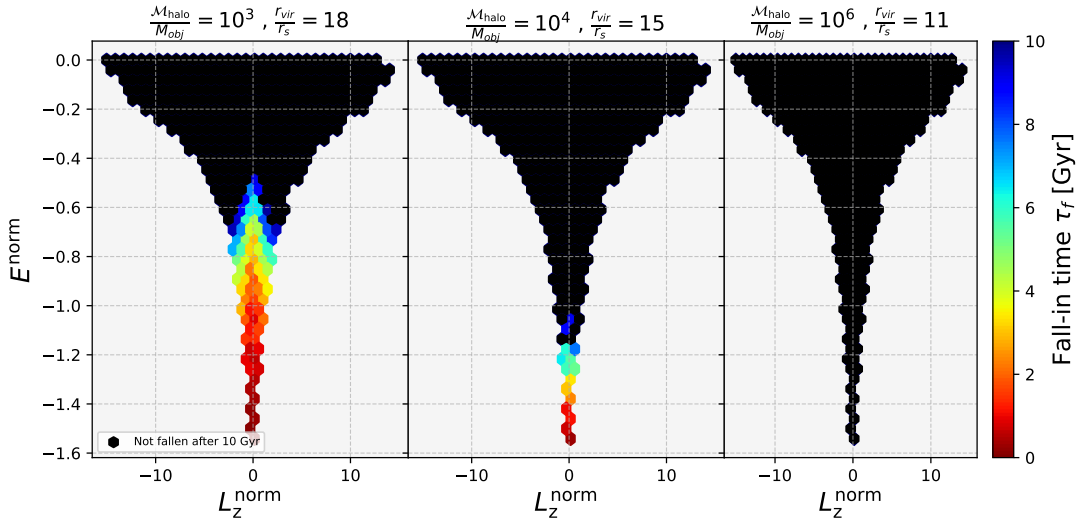

Figure 8: $E - L_z$ diagrams of GC orbits in CDM halos with different mass ratios. The quantities have been normalized by their absolute values of a circular orbit at the scale radius r_s.

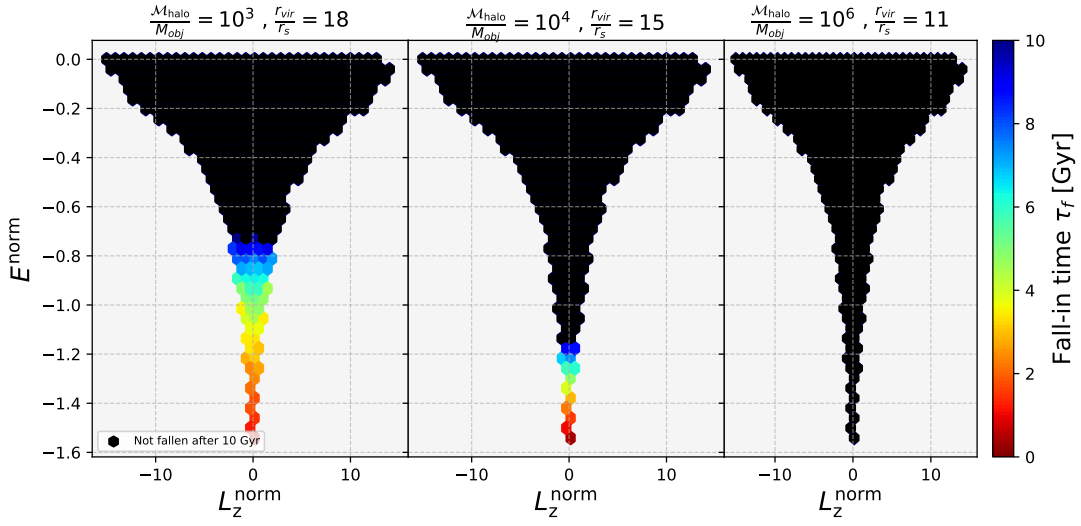

Figure 9: Same as in Figure 6 but integrated using FDM DF, with $m_{22} = 5$.

Figure 8 illustrates the impact of the halo-GC mass ratios on the orbital time of GCs that undergo dynamical friction in NFW halos. Each subplot corresponds to a different halo mass $\mathcal{M}_{\rm halo}$, then the concentration is computed using `colossus`.

We see that the more massive the halo, the less concentrated it is. This is because the virial radius $r_{\rm vir}$ increases faster than the scale radius r_s when the halo mass increases. This behavior is derived from the observations. During its history, a galaxy will merge with other galaxies,

resulting in mixing all the components, and thus, it decreases the concentration value. We observe here the effect of the mass ratio between GC $M_{\rm obj}$ and the halo $\mathcal{M}_{\rm halo}$. The dynamical friction effect decreases as the ratio increases. This effect was expected because a halo of higher mass accelerates the GCs more strongly. Then it is more difficult to lose energy due to dynamical friction. An additional effect is that the most massive galaxies are less concentrated, and then the density is lower, which decreases the dynamical friction. Another way to understand it is to look at the characteristic time for the apocenter of the orbit to change due to dynamical friction: $t_{\rm DF} = \frac{\mathcal{M}_{\rm halo}(r)}{M_{\rm obj}} t_{\rm dyn}$, where $t_{\rm dyn}$ is the orbital time (Boldrini and Bovy 2022, Binney et al. 2008). This result illustrates how dynamical friction efficiency decreases in massive galaxies. This is the reason why in massive galaxies, such as the Milky Way ($\sim 10^{12}\,{\rm M}_\odot$), there is not strong dynamical friction and why it is more efficient in dwarf galaxies.

Figure 9 shows the fall-in time of GCs in the same DM halos as in Figure 8, but with FDM DF. As in Figure 8, the concentration parameter is computed using `colossus`, with redshift $z = 0$ and halo mass $\mathcal{M}_{\rm halo}$.

We found again that the lowest-energy GCs are the first to fall and that the more massive the halo the less dynamical friction. Looking at the left panel, compared to the classical DF, the fall-in time is higher for all orbits. Furthermore, we see that there are more black areas, that is, less orbits falling within 10 Gyr. This result shows that the expected decrease of FDM on dynamical friction is effectively found. We notice that for the middle and right panels, there is no significant difference from classical DF. This is because for high mass ratios, the DF is no longer efficient in both the CDM and FDM models.

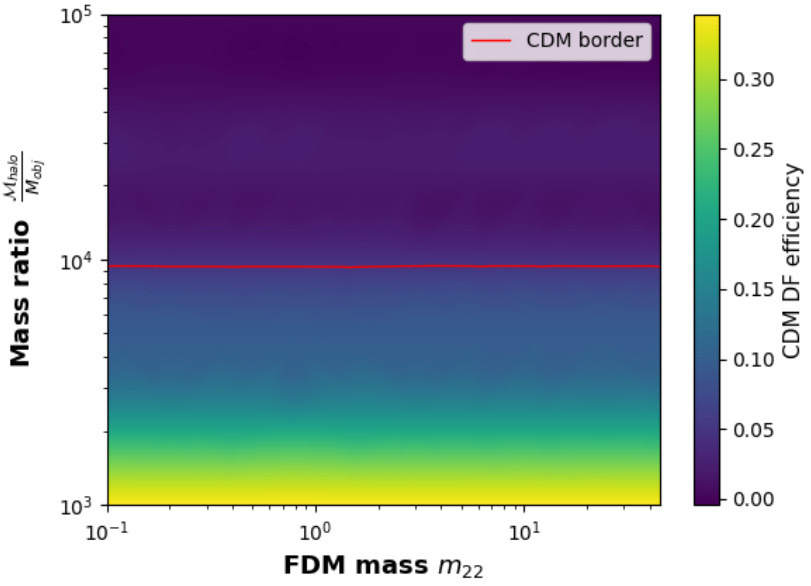

Figure 10: Dynamical friction efficiency in NFW Halo using Chandrasekhar dynamical friction. Vertical axis : halo/GC mass ratio. Horizontal axis : FDM particle mass. The red line represents the limit of 5% efficiency, calculated using the criterion discussed in the text below.

In order to have an even more general idea of the efficiency of dynamical friction to make the object fall, we decided to set, as an efficiency criterion, the relative difference between the last apocenter of an orbit which undergo dynamical friction and an orbit without DF. By computing this criterion on a significant sample of 50 orbits and taking the mean value of the results, it

provides an idea of the DF efficiency for different halo/GC mass ratios. The Figure 10 illustrates this idea.

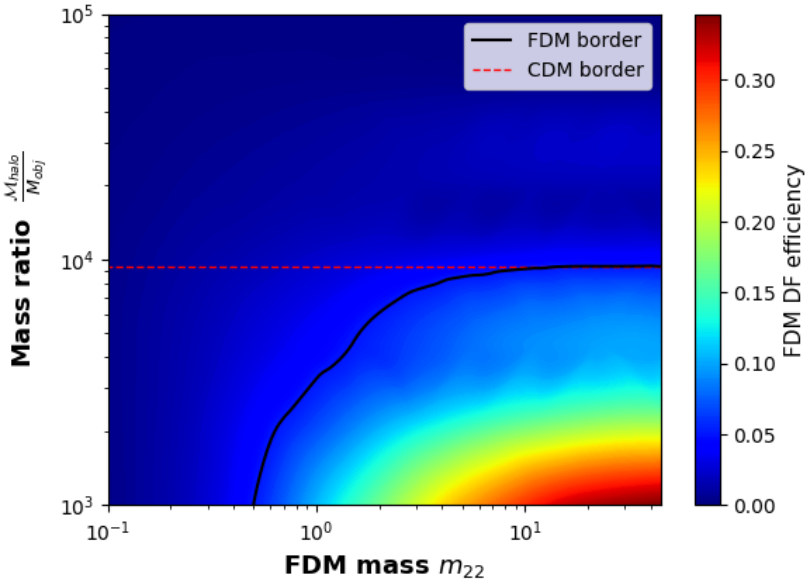

Figure 11: Dynamical friction efficiency in NFW Halo using FDM dynamical friction. Vertical axis : Halo/GC mass ratio. Horizontal axis : FDM particle mass. The solid red line represents the limit of 5% efficiency. The dashed red line represents the CDM 5% limit from Figure 10.

We notice in Figure 10 that in the CDM universe, the higher the mass ratio, the less efficient the DF. We have already shown this result in Figure 8 and we recover it here. The figure shows that above a mass ratio $\frac{\mathcal{M}_{\rm halo}}{M_{\rm obj}} \sim 10^4$, the classical dynamical friction is no longer efficient to make the globular cluster fall into the center. This result is important because it means that to observe the effect of DF, we know that we have to look to galaxies less massive than $10^4\,\mathrm{M}_\odot$, that is, dwarf galaxies.

For the semi-FDM scenario, since the mass of the FDM particle is not yet restricted, we test a range of values and look at how it modifies the dynamical friction. Afterward, we computed the orbits for different halo masses and also different FDM particle's mass $m_{22} = 0.1 - 40$. In order to have a similar plot to Figure 10, we calculated the efficiency criterion in the same way.

Figure 11 presents the efficiency map of dynamical friction as a function of the halo-to-GC mass ratio and the FDM particle mass m_{22}. As in the CDM scenario shown in Figure 10, we observe that increasing the mass ratio leads to a decrease in dynamical friction efficiency. This trend has already been highlighted in both the CDM (see Figure 8) and FDM (see Figure 9) cases.

In the FDM scenario, the efficiency of dynamical friction also depends on the value of the particle mass: the lower the particle mass, the less efficient the dynamical friction. This behavior is physically motivated, as a lower particle mass enhances quantum fluctuations, resulting in greater under-densities in the wake and thus a weaker drag force. As shown in Equation 1 and Figure 2, a lower m_{22} leads to a smaller $C_{\rm FDM}$, and consequently to a weaker dynamical friction force.

The highest efficiency is found for the lowest mass ratios and the largest particle masses. The solid red line at 5% in the figure marks the threshold for dynamical friction efficiency. We

find that for FDM particle masses m_{22} above ~ 30, the FDM dynamical friction becomes as effective as the classical DF, as illustrated in the figure. Most importantly, for FDM masses below ~ 0.45, FDM DF has no significant effect on GCs with mass $M_{\rm obj} \sim 10^6\,{\rm M}_\odot$ in any galaxy. This result is crucial, as it identifies the systems that are most relevant to investigate FDM dynamical friction.

Conclusion and discussion

Although ΛCDM is still the dominant model for describing the universe on cosmological scales, the lack of an elementary particle for dark matter suggests an incomplete understanding of the physics behind it. Furthermore, many ΛCDM predictions are still in conflict with observations (core dark matter halo, Fornax GCs). Of course, there are many different approaches to solve these deficiencies. In this work, we test an alternative model of dark matter called FDM and, more precisely, we have studied how it modifies dynamical friction in dark matter halo. This exotic dark matter model lies on the existence of an ultralight boson of $m_{\rm FDM} \sim 10^{-22}$ eV, which creates quantum interferences in the gravitational potential. This feature has several consequences on dynamics because, first, it modifies the density profile into a central region characterized by a homogeneous core, and, second, it reduces the amplitude of the drag of dynamical friction, depending on the FDM mass.

We first looked at how the classical dynamical friction is affected by the host dark matter halo's feature, such its mass and concentration, using the orbital integration code, `galpy`, and we tested all possible bound orbits for each configuration of the halo in energy-angular momentum space. We find that dynamical friction is more efficient for concentrated halos. We determined that for a mass ratio greater than 10^4, the classical dynamical friction force applied on GCs becomes negligible. The new contribution of this result is the exhaustiveness of the energy-angular momentum space, it enables to know for given initial conditions whether the GC is expected to have fallen or not.

Then we compared the effect of modifying dynamical friction using quantum treatment with FDM. We did the same test case as we did in the CDM scenario, adding a free parameter which is the FDM particle's mass m_{22}. We found that dynamical friction is no longer efficient on globular cluster for $m_{22} \sim 0.45$. For a mass higher than $m_{22} = 30$, the FDM version of dynamical friction is similar to the classical version.

To integrate the GC orbits with FDM dynamical friction, it has been necessary to develop a new extension of `galpy`, to create this particular potential. This will be added to the public code soon. We made an analytical test comparison with the code. We compared our method with the theoretical work done by Hui et al. 2017 and found that a more realistic calculation of orbital time, that is, using evolving parameters in FDM dynamical friction, leads to strong differences from the previous work. Some orbits remain in an almost stable circular orbit at low radii, an effect called "core stalling". This effect is usually caused by the density profile, but here we observed it even within the NFW halo. These results show that GC orbits are longer and more stable in an NFW halo, due to the reduction of dynamical friction. This could serve as an observable signature to constrain the nature of dark matter, particularly by observing the survival of satellites in galaxies such as Fornax.

To have a complete FDM scenario, one must change the density profile of the DM halo and use cored density profiles. This feature is expected to reduce more the dynamical friction efficiency, since the central region of the halo is less dense. In order to have more realistic scenarios, it is possible to add star and gas components in the potentials. This would increase the density in the central region. By computing the mass loss of globular cluster through tidal forces, we

could have another criterion to consider the satellite "fallen", and it would be more consistent with the observations. In addition, it is also possible to introduce an evolution of the density profiles. Finally, the new extension `FDMDynamicalFrictionForce` is in the process of being added to the public code `galpy`, with the PI of the project, Jo Bovy. All these perspectives will be implemented later on and will be the subject of a publication.

References

Binney, J. et al. *Galactic dynamics*. 2. ed. Princeton series in astrophysics. Princeton, NJ Oxford: Princeton University Press, 2008. 885 pp. ISBN: 978-0-691-13027-9 978-0-691-13026-2.

Boldrini, P. "The Cusp–Core Problem in Gas-Poor Dwarf Spheroidal Galaxies". In: *Galaxies* 10.1 (Dec. 30, 2021), p. 5. ISSN: 2075-4434. DOI: 10.3390/galaxies10010005. URL: https://www.mdpi.com/2075-4434/10/1/5 (visited on 06/12/2025).

Boldrini, P. and J. Bovy. "No globular cluster progenitors in Milky Way satellite galaxies". In: *Monthly Notices of the Royal Astronomical Society* 516.3 (Sept. 23, 2022), pp. 4560–4568. ISSN: 0035-8711, 1365-2966. DOI: 10.1093/mnras/stac2578. arXiv: 2106.09419[astro-ph]. URL: http://arxiv.org/abs/2106.09419 (visited on 06/12/2025).

Bovy, J. "galpy: A Python Library for Galactic Dynamics". In: *The Astrophysical Journal Supplement Series* 216.2 (Feb. 3, 2015), p. 29. ISSN: 1538-4365. DOI: 10.1088/0067-0049/216/2/29. arXiv: 1412.3451[astro-ph]. URL: http://arxiv.org/abs/1412.3451 (visited on 04/07/2025).

Chandrasekhar, S. "Dynamical Friction. I. General Considerations: the Coefficient of Dynamical Friction." In: *The Astrophysical Journal* 97 (Mar. 1943), p. 255. ISSN: 0004-637X, 1538-4357. DOI: 10.1086/144517. URL: http://adsabs.harvard.edu/doi/10.1086/144517 (visited on 01/13/2025).

Cole, D. R. et al. "The mass distribution of the Fornax dSph: constraints from its globular cluster distribution". In: *Monthly Notices of the Royal Astronomical Society* 426.1 (Oct. 11, 2012), pp. 601–613. ISSN: 00358711. DOI: 10.1111/j.1365-2966.2012.21885.x. arXiv: 1205.6327[astro-ph]. URL: http://arxiv.org/abs/1205.6327 (visited on 05/20/2025).

Diemer, B. "COLOSSUS: A python toolkit for cosmology, large-scale structure, and dark matter halos". In: *The Astrophysical Journal Supplement Series* 239.2 (Dec. 1, 2018), p. 35. ISSN: 0067-0049, 1538-4365. DOI: 10.3847/1538-4365/aaee8c. arXiv: 1712.04512[astro-ph]. URL: http://arxiv.org/abs/1712.04512 (visited on 04/28/2025).

Hu, W. et al. "Fuzzy Cold Dark Matter: The Wave Properties of Ultralight Particles". In: *Physical Review Letters* 85.6 (Aug. 7, 2000), pp. 1158–1161. ISSN: 0031-9007, 1079-7114. DOI: 10.1103/PhysRevLett.85.1158. URL: https://link.aps.org/doi/10.1103/PhysRevLett.85.1158 (visited on 06/05/2025).

Hui, L. et al. "Ultralight scalars as cosmological dark matter". In: *Physical Review D* 95.4 (Feb. 28, 2017), p. 043541. ISSN: 2470-0010, 2470-0029. DOI: 10.1103/PhysRevD.95.043541. URL: https://link.aps.org/doi/10.1103/PhysRevD.95.043541 (visited on 01/13/2025).

Lancaster, L. et al. "Dynamical Friction in a Fuzzy Dark Matter Universe". In: *Journal of Cosmology and Astroparticle Physics* 2020.1 (Jan. 2, 2020), pp. 001–001. ISSN: 1475-7516. DOI: 10.1088/1475-7516/2020/01/001. arXiv: 1909.06381[astro-ph]. URL: http://arxiv.org/abs/1909.06381 (visited on 01/13/2025).

Lee, J.-W. et al. "Minimum mass of galaxies from BEC or scalar field dark matter". In: *Journal of Cosmology and Astroparticle Physics* 2010.1 (Jan. 4, 2010), pp. 007–007. ISSN: 1475-7516. DOI: 10.1088/1475-7516/2010/01/007. URL: https://iopscience.iop.org/article/10.1088/1475-7516/2010/01/007 (visited on 06/16/2025).

Navarro, J. F. et al. "The Structure of Cold Dark Matter Halos". In: *The Astrophysical Journal* 462 (May 1996), p. 563. ISSN: 0004-637X, 1538-4357. DOI: 10.1086/177173. arXiv: astro-ph/9508025. URL: http://arxiv.org/abs/astro-ph/9508025 (visited on 04/07/2025).

– "A Universal Density Profile from Hierarchical Clustering". In: *The Astrophysical Journal* 490.2 (Dec. 1997), pp. 493–508. ISSN: 0004-637X, 1538-4357. DOI: 10.1086/304888. URL: https://iopscience.iop.org/article/10.1086/304888 (visited on 06/05/2025).

Planck Collaboration et al. "*Planck* 2018 results: VI. Cosmological parameters". In: *Astronomy & Astrophysics* 641 (Sept. 2020), A6. ISSN: 0004-6361, 1432-0746. DOI: 10.1051/0004-6361/201833910. URL: https://www.aanda.org/10.1051/0004-6361/201833910 (visited on 03/24/2025).

Riess, A. G. et al. "Observational Evidence from Supernovae for an Accelerating Universe and a Cosmological Constant". In: *The Astronomical Journal* 116.3 (Sept. 1998), pp. 1009–1038. ISSN: 00046256. DOI: 10.1086/300499. URL: https://iopscience.iop.org/article/10.1086/300499 (visited on 03/24/2025).